JLAB USER GROUP

Jefferson Lab PAC13
Proposal Cover Sheet

This document must be received by close of business Thursday, **December 18, 1997** at:

Jefferson Lab
User Liaison Office,
Mail Stop 12B
12000 Jefferson Avenue
Newport News, VA
23606

Experimental Hall: A

Days Requested for Approval: 16

☒ **New Proposal Title:** The GDH Sum Rule and the Spin Structure of ^{3}He and the Neutron Using Nearly Real Photons.

☐ **Update Experiment Number:**

☐ **Letter-of-Intent Title:**

(Choose one)

Proposal Physics Goals
Indicate any experiments that have physics goals similar to those in your proposal.

To Measure the GDH sum rule and the spin structure for ^{3}He and the neutron at $0.02\ (GeV/c)^2 < Q^2 < 0.5\ (GeV/c)^2$. To study the slope of the GDH at real photon point and to extrapolate to real photon point. Also to provide a test of how good the assumption that polarized ^{3}He is approximate a polarized neutron target.

Approved, Conditionally Approved, and/or Deferred Experiment(s) or proposals:

Based on LOI-97-003

Contact Person

Name: JIAN-PING CHEN
Institution: JEFFERSON LAB
Address: 12H, C124
Address: 12000 JEFFERSON AVE.
City, State, ZIP/Country: NEWPORT NEWS, VA 23606
Phone: (757) 269-7413 **Fax:** (757) 269-5235
E-Mail: JPCHEN@JLAB.ORG

JLab Use Only

Receipt Date: 12/18/97 PR 97-110

By: gp

HAZARD IDENTIFICATION CHECKLIST

JLab Proposal No.: _____ Date: 12/18/97
(For CEBAF User Liaison Office use only.)

Check all items for which there is an anticipated need.

Cryogenics
- _____ beamline magnets
- ✓ analysis magnets
- _____ target
  - type: _____
  - flow rate: _____
  - capacity: _____

Electrical Equipment
- _____ cryo/electrical devices
- _____ capacitor banks
- _____ high voltage
- _____ exposed equipment

Radioactive/Hazardous Materials
List any radioactive or hazadorous/ toxic materials planned for use:
_____
_____
_____
_____

Pressure Vessels
- _____ inside diameter
- _____ operating pressure
- _____ window material
- _____ window thickness

Flammable Gas or Liquids
- type: _____
- flow rate: _____
- capacity: _____

Drift Chambers
- type: _____
- flow rate: _____
- capacity: _____

Other Target Materials
- ___ Beryllium (Be)
- ___ Lithium (Li)
- ___ Mercury (Hg)
- ___ Lead (Pb)
- ___ Tungsten (W)
- ___ Uranium (U)
- ___ Other (list below)

_____
_____

Vacuum Vessels
- _____ inside diameter
- _____ operating pressure
- _____ window material
- _____ window thickness

Radioactive Sources
- _____ permanent installation
- _____ temporary use
- type: _____
- strength: _____

Large Mech. Structure/System
- _____ lifting devices
- _____ motion controllers
- _____ scaffolding or
- _____ elevated platforms

Lasers
- type: Diode
- wattage: 100 W
- class: IV

Installation:
- _____ permanent
- ✓ temporary

Use:
- _____ calibration
- _____ alignment

for polarized ^{3}He target

Hazardous Materials
- ___ cyanide plating materials
- ___ scintillation oil (from)
- ___ PCBs
- ___ methane
- ___ TMAE
- ___ TEA
- ___ photographic developers
- ___ other (list below)

_____
_____

General:

Experiment Class:
- ✓ Base Equipment
- _____ Temp. Mod. to Base Equip.
- _____ Permanent Mod. to Base Equipment
- ✓ Major New Apparatus

Other: Polarized ^{3}He target
Septum Magnets

LAB RESOURCES LIST

JLab Proposal No.: _____ Date 12/18/97
(For JLab ULO use only.)

List below significant resources — both equipment and human — that you are requesting from Jefferson Lab in support of mounting and executing the proposed experiment. Do not include items that will be routinely supplied to all running experiments such as the base equipment for the hall and technical support for routine operation, installation, and maintenance.

Major Installations *(either your equip. or new equip. requested from JLab)*

Install polarized ^{3}He target

Install Septum Magnets

New Support Structures:

Data Acquisition/Reduction

Computing Resources:

New Software:

Major Equipment

Magnets: Septum Magnets

Power Supplies:

Targets: Polarized ^{3}He target

Detectors:

Electronics:

Computer Hardware:

Other:

Other:

BEAM REQUIREMENTS LIST

JLab Proposal No.: _____ Date: 12/18/97

Hall: A Anticipated Run Date: Late 1999, to early 2000 PAC Approved Days: _____

Spokesperson: JIAN-PING CHEN, Gordon Cates Franco Ciaraldi Hall Liaison: JIAN-PING CHEN
Phone: (757) 269-7413
E-mail: JPCHEN@JLAB.ORG

List all combinations of anticipated targets and beam conditions required to execute the experiment. (This list will form the primary basis for the Radiation Safety Assesment Document (RSAD) calculations that must be performed for each experiment.)

Condition No.	Beam Energy (MeV)	Mean Beam Current (μA)	Polarization and Other Special Requirements (e.g., time structure)	Target Material (use multiple rows for complex targets — e.g., w/windows)	Material Thickness (mg/cm²)	Est. Beam-On Time for Cond. No. (hours)
1	1645	5	80% polarized	pol. ^{3}He target	50 mg/cm²	28
2	2045	5	v	v	v	12
3	3045	10	v	v	v	42
4	4045	10	v	v	v	14
5	5045	15	v	v	v	52
6	6045	15	v	v	v	54

The beam energies, E_{Beam}, available are: $E_{Beam} = N \times E_{Linac}$ where N = 1, 2, 3, 4, or 5. E_{Linac} = 800 MeV, i.e., available E_{Beam} are 800, 1600, 2400, 3200, and 4000 MeV. Other energies should be arranged with the Hall Leader before listing.

PAC12 Report

Appendix E

Letter-of-Intent: LOI-97-003

Spokespersons: J. P. Chen

Title: The GDH Sum Rule and the Spin Structure of ^{3}He and the Neutron using Nearly Real Photons

The installation of a pair of septum magnets for the Hall A spectrometers allows a decrease in the value of the scattering angle to $\theta = 6°$. This allows measurements of electron scattering data at very small Q^2 near the photon point. This letter-of-intent proposes to study the Q^2 dependence of the Drell-Hearn-Gerasimov sum rule for ^{3}He near the real photon point.

The PAC finds this LOI to be of significant interest. The data would provide information on a region extending from threshold to beyond the resonances. The comparison of these data to similar measurements planned at Jefferson Lab on the deuteron will provide an important cross check of the interpretation of these data for the understanding of the neutron spin structure function.

The PAC encourages the collaboration to submit a proposal.

(A New Proposal to TJNAF PAC13)
The GDH Sum Rule and the Spin Structure of ^{3}He and the Neutron using Nearly Real Photons

Todd Averett, K. Bega, B. Carr, B.W. Filippone, E. Goldberg, E. Hughes,
S. Jensen, C. Jones, R.D. McKeown, D. Pripstein
CALIFORNIA INSTITUTE OF TECHNOLOGY

H. X. He, X. D. Liu, Z. X. Sun, J. Yuan, X. F. Zhu
China Institute of Atomic Energy, China

P. Markowitz
FLORIDA INTERNATIONAL UNIVERSITY

E. CisBani, S. Frullani, F. Garibaldi (Co-spokesperson), M. Iodice, G. Salme, G. Urciuoli
INFN SEZIONE SANITA, ITALY

E. de Leo, R. Perrino
INFN SEZIONE LECCE, ITALY

C. Ciofi degli Atti, S. Scopetta
INFN SEZIONE PERUGIA, ITALY

V. Burkert, J.P. Chen (Spokesperson), E. Chudakov, J. Gomez, O. Hansen, K. de Jager,
M. Kuss, M. Liang, J. LeRose, R. Michaels, S. Nanda, P. Rutt, A. Saha, B. Wojtsekhowski
THOMAS JEFFERSON NATIONAL ACCELERATOR FACILITY

A. Afanasev
JEFFERSON LAB AND NORTH CAROLINA CENTRAL UNIVERSITY

C. Corianó, A. Gasparian, J. Goity
JEFFERSON LAB AND HAMPTON UNIVERSITY

B. Anderson, G.G. Petratos, D. Prout, R. Suleiman, J. Watson
KENT STATE UNIVERSITY

D. Dale, W. Korsch
UNIVERSITY OF KENTUCKY

C. C. Chang
MARYLAND UNIVERSITY

H. Gao, T. Black, W. Xu
MASSACHUSETTS INSTITUTE OF TECHNOLOGY

A. Deur, C. Hyde-Wright, K. McCormick
OLD DOMINION UNIVERSITY

G.D. Cates(Co-spokesperson), G. S. Corrado, B. Humensky, I. Kominis, K. Kumar, G. W. Miller, T. Pavlin
PRINCETON UNIVERSITY

C. Glashausser, R. Gilman, G. Kumbartzki, J. McIntyre, R.D. Ransome
RUTGERS UNIVERSITY

P.A. Souder, R. Holmes, R.Kahl, J. Yeh
SYRACUSE UNIVERSITY

L. Auerbach, Z.-E. Meziani, M. Schnee, K. Slifer
TEMPLE UNIVERSITY

K. Maeda, T. Saito
TOHOKU UNIVERSITY, JAPAN
(December 18, 1997)

Abstract

We propose to measure asymmetries (and cross section differences) for polarized electron scattering off polarized ^{3}He at very low Q^2 range of 0.02 to 0.5 $(GeV/c)^2$ by using the new Hall A septum magnets. The Q^2 dependence of the GDH sum rule will be studied at this low Q^2 range. The slope of the GDH sum rule at Q^2 near zero will be measured and a reasonable extrapolation to the real photon point can be obtained. The slope of the GDH sum rule at $Q^2 = 0$ predicted by Chiral Perturbation Theory is very different from that predicted by quark models and resonance saturation models based on partial wave analysis.

Spin structure functions will be measured from the threshold region, through the quasielastic region to the resonance region and beyond. Since no double polarization measurement has previously been performed or planned at such a low Q^2 range, the measurements will add an essential data set to constrain our understanding of ^{3}He and the neutron spin structure, and will enable a better study of the resonances. The comparison of ^{3}He and the neutron GDH sum rule will be used to study how good is the assumption that the polarized ^{3}He target is almost a polarized neutron target, and to test ^{3}He models.

I. INTRODUCTION

A. Gerasimov-Drell-Hearn Sum Rule

The Gerasimov-Drell-Hearn (GDH) sum rule [1] relates the total cross section of circularly polarized photons on longitudinally polarized nucleons to the anomalous magnetic moment of the nucleon:

$$\int_{thr}^{\infty}(\sigma_{1/2}-\sigma_{3/2})\frac{d\nu}{\nu}=-2\pi^2\alpha\frac{\kappa^2}{m^2} \tag{1}$$

where $\sigma_{1/2}$ and $\sigma_{3/2}$ are the total cross sections for hadron photoproduction on nucleons in the helicity 1/2 and 3/2 states, ν is the laboratory photon energy, κ is the anomalous magnetic moment and m is the mass of the nucleon. The lower limit of the integration is the pion photoproduction threshold.

The GDH sum rule follows from the dispersion relation for forward Compton scattering along with the optical theorem and low energy theorem. The forward Compton scattering amplitude may be written in terms of two scalar invariant functions of ν:

$$f(\nu)=f_1(\nu)\vec{\epsilon}'^{*}\cdot\vec{\epsilon}+\nu f_2(\nu)i\vec{\sigma}\cdot\vec{\epsilon}'^{*}\times\vec{\epsilon} \tag{2}$$

where $\vec{\epsilon}$ and $\vec{\epsilon}'$ are the transverse polarization vectors of the incident and forward-scattered photon, respectively. Causality implies analyticity of f_2 which allows us to write the dispersion relation for the forward amplitude without subtraction:

$$\mathrm{Re}f_2(\nu)=\frac{2\nu}{\pi}\mathrm{P}\int_0^{\infty}d\nu'\frac{\mathrm{Im}f_2(\nu')}{\nu'^2-\nu^2}. \tag{3}$$

Unitarity can be expressed in the optical theorem:

$$\mathrm{Im}f_2(\nu)=\frac{\nu}{8\pi}(\sigma_{1/2}-\sigma_{3/2}) \tag{4}$$

The low energy theorem [2], which comes from gauge invariance and relativity, informs us that

$$f_2(0)=-\frac{\alpha\kappa^2}{2m^2}. \tag{5}$$

Combining the above equations, the GDH sum rule follows immediately. The no-subtraction assumption ($\mathrm{Re}(f_2(\infty))=0$) and that the cross section difference falls off with energy faster than $1/\ln(\nu)$ could be open to 'reasonable' question. The generality of the input assumption suggests very strongly that the sum rule should be verified, which has become possible now with the technical development in polarized beams, polarized targets and the new detection capabilities at TJNAF.

Because of the $1/\nu$ weighting in the integrals, and that the resonances contribute most of the strength to the sum rule, single pion photoproduction is expected to have a sizeable contribution (dominant at low energy). Using the results of multipole analyses of the existing (mostly unpolarized) data, Karliner [3] and more recently Workman and Arndt [4], Burkert and Li [5] have computed the single pion contribution to the GDH sum rule for the proton

and the neutron, with some estimates of the inelastic contribution included. These values are compared to the GDH prediction in table 1. Also listed are the values calculated based on an extended algebra model [8]. In the extended algebra calculation, the GDH sum rule is modified by extending the assumption of the 'no-subtraction' dispersion relation to have an additional term. It is of particular interest to notice that the proton-neutron sum rule (which is equivalent to isoscalar-isovector interference sum rule) is of different sign from the partial wave analysis results, and far from saturation by the existing calculation up to 1.8 GeV. If the partial-wave analysis results are right, it would require a prominent structure above 1.8 GeV overcoming the $1/\nu$ factor to make the partial-wave analysis result agree with the GDH prediction. But a similar calculation on proton-neutron's spin-dependent polarizability which has a $1/\nu^3$ factor agrees with the relativistic 1-loop chiral calculations. This indicates that either both the 2-loop correction for the polarizability is large and the existing multipole analysis are wrong or the GDH sum rule needs to be modified [6]. It will be of great interest to experimentally test the GDH rum rule on both proton and neutron.

Table 1. Various Predictions for GDH sum

-	GDH(p)	GDH(n)	GDH(p-n)
GDH sum rule	-204.5 μb	-232.8μb	28.3μb
Extended Current Algebra	-294 μb	-185μb	-109μb
Analysis by Karliner	-261 μb	-183 μb	-78 μb
Analysis by Workman and Arndt	-257 μb	-189 μb	-68 μb
Analysis by Burkert and Li	-203 μb	-125 μb	-78μb

There are some recent theoretical efforts [7] provide extensive discussions on the subject of the GDH sum rule, including discussions of the validity of the no-subtraction hypothesis, the consequences of the GDH sum rule for our understanding of the nucleon structure, and the use of the strange anomalous moments to reconcile the GDH with the partial wave analysis of the pion-photoproduction data. Two planned TJNAF experiments (E91-015 [24] and E94-117 [25]) will use polarized real photon on polarized Hydrogen and Deuterium targets using CLAS to study part of the GDH sum rule. Similar studies are also planned at LEGS [26], Bonn, MAINZ [27], and Grenoble [28].

The difficulty associated with the real photon experiments is that to measure the total absorption cross section, one needs to detect particles at all the solid angles, which is often not possible due to the incomplete coverage of the detectors. Inclusive electron scattering would be an attractive alternative method to measure the GDH sum rule, provided one can measure at very low Q^2 and extrapolate to $Q^2 = 0$. The extrapolation will be reasonable if the slope of the GDH sum at the $Q^2 = 0$ point is smooth and can be measured.

B. Generalized Gerasimov-Drell-Hearn Sum Rule With Virtual Photons

The recent interest in the GDH sum rule was also raised by Anselmino et al. [9] and others [10] when they suggested a connection between the GDH sum rule and the spin structure function g_1 of the nucleon, in an attempt to understand the nucleon 'spin crisis' raised by the results of an EMC experiment [11] combined with early SLAC experiments [12]. Recent results on the spin structure functions of the nucleons, at high $< Q^2 >$ (> 2 GeV/c^2),

from the SMC [13], SLAC E142, E143, E154 and E155 [14] and HERMES [15] experiments confirmed the Bjorken sum rule. The result on the integral of the spin structure function $\Gamma_p = 0.136 \pm 0.015$ and various theoretical analyses lead to the conclusion that degrees of freedom other than the valence quarks have important contributions to the proton's spin. The results also show the great importance of the Q^2 dependence of the spin structure functions. The GDH sum rule gives the prediction at $Q^2 = 0$ (real photon) point which can be related to the spin structure functions in electron (or muon) scattering by

$$\sigma_{TT'} = \frac{\sigma_{3/2} - \sigma_{1/2}}{2} = -\frac{4\pi^2 \alpha m}{(1-x)}(G_1(Q^2,\nu) - 2xG_2(Q^2,\nu)). \tag{6}$$

where

$$G_1 = \frac{m^2 g_1}{\nu}, \qquad G_2 = \frac{m^4 g_2}{\nu^2}. \tag{7}$$

In both cases of deep-inelastic scattering and real photo-absorption, the contribution of the second term vanishes and $\sigma_{3/2} - \sigma_{1/2}$ is expressed simply in terms of G_1. The generalized GDH sum can be defined as follows:

$$I(Q^2) = -\frac{m^2}{4\pi\alpha}\int_{thr}^{\infty}\frac{d\nu}{\nu}(1-x)\sigma_{TT'}(Q^2,\nu) = \frac{2m^2}{Q^2}\int_0^1 dx[g_1(Q^2,x) - \frac{4x^2m^2}{Q^2}g_2(Q^2,x)] \tag{8}$$

which at $Q^2 = 0$ is given by the GDH sum rule:

$$I(0) = \frac{m^2}{8\pi^2\alpha}\int_{thr}^{\infty}(\sigma_{1/2} - \sigma_{3/2})\frac{d\nu}{\nu} = -\frac{\kappa^2}{4}. \tag{9}$$

The question of main current interest is the behavior of the integral $I(Q^2)$ in the low and intermediate regime of Q^2. Determining and understanding this behavior at intermediate regime of Q^2 are the main goal of three approved TJNAF experiments: E91-023 (Hall B) [29] (proton target),E93-009 (Hall B) [30] (Deuteron), E94-010 (Hall A) [31] (^3He). These experiments will cover the domain 0.2 GeV$^2 < Q^2 <$ 2.0 GeV^2, measuring the spin structures of the proton and the neutron in the resonance region. Similar studies were also proposed at some other labs [16]. As the discussion below will show, there are important open issues below Q^2 of 0.2 GeV^2, and experiments in that range will be of great significance.

Theoretically, the knowledge of $I(Q^2)$ at low and medium Q^2 is uncertain. One prediction is based on the resonance saturation model of Burkert and Li [5]. In this model, the helicity cross sections, or equivalently the two spin dependent structure functions, are obtained by considering the electro-production of baryonic resonances. Experimentally obtained photo-couplings are used at the photon point, and when $Q^2 > 0$ form factors are included. This model predicts a dramatic change of behavior of $I(Q^2)$ below Q^2 of 0.15 GeV^2: A turn-around at Q^2 around 0.06 GeV^2 and a negative slope at Q^2 near zero. In this model, the dominant contribution to $I(Q^2)$ is by the $M1$ production of the $\Delta(1232)$ isobar. Its photocouplings and, to a lesser extent, its form factor for the $M1$ transition, are well known. With just this resonance included it is possible to see the evolution and the turn-around. Also, the $\Delta(1232)$ alone gives the large share to the GDH sum rule. The contributions from the rest of the resonances is less certain. While, on general grounds of multipole analysis the

signs of the contributions due to different resonances can be determined, their magnitudes are only roughly known. Another important issue is the πN continuum contribution. This contribution to the slope of $I(Q^2)$ at Q^2 near zero is found in a simple model [17] to be positive. But, the combined contribution from the πN continuum and the resonances is still negative, with a turn-around at about 0.06 GeV^2 However, this is not the conclusion of a Chiral Perturbation Theory analysis [18]. The slope of $I(Q^2)$ at Q^2 near zero was predicted by the Chiral Perturbation Theory analysis, where a large positive slope was found. Clearly, the current theoretical understanding is not sufficient to make a firm prediction of the low Q^2 behavior.

The different predictions of the slope at Q^2 near zero can be settled with measurements at Q^2 below the predicted turn around point. Also it has been shown [17] that the very low Q^2 region is a sensitive region to study the resonance structure. The very low Q^2 measurements of the $I(Q^2)$ can be used to determine the slope at Q^2 near zero and then can be extrapolated to $Q^2 = 0$, the real photon point. Due to the difficulty involved in the real photon total absorption measurements and the simplicity of inclusive electron scattering, the very low Q^2 measurements of the $I(Q^2)$ are attractive alternative to measure the GDH sum rule at the real photon point. However, it is clear that with a turn-around at $Q^2 \approx 0.06(GeV/c)^2$ as predicted by the resonance saturation model, one can not extrapolate with the data (of the presently approved experiments) at Q^2 range of 0.2 to 2 (GeV/c)^2 to real photon point. To have a reasonable extrapolation, one needs to make measurements to significantly lower than the turn around point.

With the new design of the septum magnets in Hall A, angles as small as 6° can be reached. With the small angle capability, we can access a Q^2 range as low as 0.02 (GeV/c)^2, significantly below the predicted turn around point. We will be able to measure the region around the predicted turn around point and to measure the slope at Q^2 near zero, and to make a reasonable extrapolation to the real photon point.

C. Gerasimov-Drell-Hearn Sum Rule for Nuclei

The GDH sum rule also applies to nuclei. The GDH sum rule relates the total cross section of circularly polarized photons on a longitudinally polarized nucleus to the anomalous magnetic moment of the nucleus:

$$\int_{thr}^{\infty}(\sigma_A - \sigma_P)\frac{d\nu}{\nu} = -4\pi^2\frac{\mu_A^2}{J} \tag{10}$$

where σ_P and σ_A are the total photo-absorption cross sections on nucleus, with nuclear spin J parallel and antiparallel to the photon polarization, $\mu_A = \mu - JQ\bar{h}/M$ is the anomalous magnetic moment of the nucleus, where Q and M are the charge and mass of the nucleus. The lower limit of the integration is the photo-nuclear disintegration threshold.

For ^{3}He, $\mu = -2.128\mu_0$, spin is 1/2, the threshold is about 5.9 MeV, and the sum rule is $496\mu b$. If the polarized ^{3}He is almost a polarized neutron target, then the integration from the pion threshold to infinite should be almost equal to the neutron sum rule ($233\mu b$) and from the disintegration threshold to the pion threshold should be approximately equal to the difference of the ^{3}He to the neutron sum rule ($263\mu b$). The measurements from the disintegration threshold to the pion threshold can be used to study how good is the

assumption that polarized ^{3}He is almost a polarized neutron target, and therefore to test ^{3}He models.

II. EXPERIMENTAL SETUP AND PROPOSED MEASUREMENTS

A. Septum Magnets

Two septum magnets will be added to the Hall A HRS2 spectrometers to allow measurements at more forward angles (smaller than 12.5° , the minimum achievable now, down to 6°). The magnets have been designed for hypernuclear electroproduction experiments. It has been shown ([32]) that it is possible to add septum magnets without major modifications of the characteristics of the spectrometers (namely the solid angle and the energy resolution). The angular acceptance will be $\sim 3.7msr$, and the momentum resolution will be $< 2. \times 10^{-4}$. Moreover, the aim is to have a general purpose device, so particles scattered at the new minimum angle should also reach momenta as high as the maximum central momentum analyzable by the HRS2 (4 GeV/c), while keeping the possibility of varying the angle from 6° to 12.5°, the "normal" HRS setup minimum angle.

In Table 2 we summarize the desired performances of the new HRS + septum spectrometer.

Table 2 Performance Requirements

	HRS	HRS(achieved)	Septum
Angular acceptance	7.2 msr	6 msr	3.7
Momentum resolution	1.0×10^{-4}	2.0×10^{-4}	2.0×10^{-4}
Minimum scattering angle	12.5°	12.5°	6°
Momentum Range	0.4-4 GeV/c	0.4-4 GeV/c	0.4-4 GeV/c

Physically, the first quadrupole ($Q1$) of the spectrometers cannot be moved closer than 12.5° to the beam without hitting the beam pipe. So the target will be moved upstream a suitable distance and a horizontal-bending septum magnet will be inserted upstream of the the spectrometers in such a way that the target seems to be situated on the optical axis of the two spectrometers (Figs.1,2).

In Table 3 we summarize the dimensions of the septum.

Table 3 Septum Dimensions

Length *	88. cm
Height of the gap	25. cm
Width of gap entrance edge	10.4 cm
Width of gap exit edge	18.4 cm
Angular acceptance	4.7 msr
Magnetic length	84. cm

(* length includes length of the coils outside the yoke)

Taking into account the limited space available for the septum (about 1.5 m along the beam axis), the required aperture width, and the desired product $B \cdot l = 2.4$ T-m, it can be shown that a magnet with warm coils saturates and therefore does not satisfy the conditions. Therefore, the option of two independent iron-shaped field SC dipoles was chosen as basic concept for the design.

A conceptual design of the septa fulfilling completely the aforementioned characteristics has been completed. In Table 4 we report the septum parameters that depend on momentum and scattering angle of detected particles. P is the scattered particle momentum, θ is the scattering angle, β is the horizontal bending angle of the septum magnet, the magnetic field (in the region of constant field) and field integral over the path are B_0 and $B \cdot dl$. R is the horizontal radius of curvature for the septum magnet.

Table 4 Septum Parameters

P	θ	β	R	$B \cdot dl$	B_0
GeV/c	degrees	degrees	cm	Tesla-m	Tesla
2	6	6.5	740.8	0.76	0.9
2	12.5	11.9	404.6	1.39	1.65
4	6	6.5	740.8	1.51	1.8
4	12.5	11.9	404.6	2.89	3.3

The stray field generated by the septa is shown in fig. 3 (The center of the target is located at $z > 158$). Its integral along the beam pipe is 0.1T*m. To compensate the particle trajectory deflection along the beam pipe a corrector coil will be added as shown in fig. 4. The stray field in the target region is at the order of 20 gauss. Calculations show that with 0.5 mm of mu metal shielding, the stray field gradient at the target region can be reduced to below the acceptable level (< 30 mG/cm). Use of field clamping with correction coils can also reduce the field gradient to below the acceptable level.

Funding for the Septum has been secured by the INFN (Italian) group. The magnets should be ordered by early 1998, and installed and commissioned in early 1999. Note that there is already one approved Hall A hypernuclear experiment [33] will use the Septum magnets.

Possible sources of background in the detector include neutrons, multiply scattered electrons and hadrons, and "junk" created by photons and electrons from the target which interact with the pole faces of the magnet and produce a spray which is directed toward the detectors. The simplest way to control these sources of background are through shielding and baffling. The data available from Hall A commissioning suggest the shielding is adequate. Baffling is being done for this experiment actively through the use of the magnetic fields. Low energy particles are swept away by first the septum (horizontally) and then the dipole (vertically). The septum setup will therefore have reduced backgrounds compared to the normal running situation in Hall A, and there is no problem foreseen with backgrounds.

B. Polarized Electron Beam

Given the technical developments currently achieved with strained GaAs cathodes at SLAC and bench tests at JLab, high electron polarization (80%) is expected to be available

at TJNAF in 1998. We assume in this proposal the achievable electron polarization at TJNAF is 80%. Beam current in the range of 1-15 μA will be used for the proposed measurements. The polarization of the beam will be measured with the Hall A Møller and/or the Compton polarimeter.

C. The Spin-Exchange Polarized ^{3}He Target

The polarized target will be based on the principle of spin exchange between optically pumped alkali-metal vapor and noble-gas nuclei [34]. The design will be similar in many ways to that used in E-142, an experiment at SLAC to measure the spin dependent structure function of the neutron [14]. A central feature of the target will be sealed glass target cells, which will contain a ^{3}He pressure of about 10 atmospheres. As shown in Figure 5, the target cells will have two chambers, an upper chamber in which the spin exchange takes place, and a lower chamber, through which the electron beam will pass. In order to maintain the appropriate number density of alkali-metal (Rb) the upper chamber will be kept at a temperature of 170–200°C using an oven constructed of the high temperature plastic Torlon. With a density of 2.5×10^{20} atoms/cm^3, and a lower cell length of 40 cm, the target thickness will be 1.0×10^{22} atoms/cm^2. The target is currently being constructed for several approved experiments in Hall A. We plan to use this target for the proposed measurements without any major upgrade or change. We describe below in detail some features of the target.

1. Operating Principles

The time evolution of the ^{3}He polarization can be calculated from a simple analysis of spin-exchange and ^{3}He nuclear relaxation rates [35]. Assuming the ^{3}He polarization $P_{^3He} = 0$ at $t = 0$,

$$P_{^3He}(t) = < P_{Rb} > \left(\frac{\gamma_{SE}}{\gamma_{SE} + \Gamma_R}\right)\left(1 - e^{-(\gamma_{SE}+\Gamma_R)t}\right), \tag{11}$$

where γ_{SE} is the spin-exchange rate per ^{3}He atom between the Rb and ^{3}He, Γ_R is the relaxation rate of the ^{3}He nuclear polarization through all channels other than spin exchange with Rb, and P_{Rb} is the average polarization of a Rb atom. Likewise, if the optical pumping is turned off at $t = 0$ with $P_{^3He} = P_0$, the ^{3}He nuclear polarization will decay according to

$$P_{^3He}(t) = P_0 e^{-(\gamma_{SE}+\Gamma_R)t}. \tag{12}$$

The spin exchange rate γ_{SE} is defined by

$$\gamma_{SE} = < \sigma_{SE} v > [Rb]_A, \tag{13}$$

where, $< \sigma_{SE} v >= 1.2 \times 10^{-19}$ cm^3/sec is the velocity-averaged spin-exchange cross section for Rb–^{3}He collisions [35-37] and $[Rb]_A$ is the average Rb number density seen by a ^{3}He atom. Our target will be designed to operate with $1/\gamma_{SE} = 8$ hours.

From Eq. (12) it is clear that there are two things we can do to get the best possible ^{3}He polarization — maximize γ_{SE} and minimize Γ_R. But from Eq. (12) it is also clear

that maximizing γ_{SE} means increasing the alkali-metal number density, which in turn means more laser power. The number of photons needed per second must compensate for the spin relaxation of Rb spins. In order to achieve $1/\gamma_{SE} = 8$ hours, which is a a faster time constant that was typically achieved at SLAC, we expect to need about 50 Watts of usable laser light at a wavelength of 795 nm. We will say more about the source of laser light below.

The rate at which polarization is lost, which is characterized by Γ_R, will have four principle contributions. An average electron beam current of about 10 μA will result in a depolarization rate of $\Gamma_{beam} = 1/45$ hours [36]. Judging from experience at SLAC, we can produce target cells with an intrinsic rate of $\Gamma_{cell} = 1/50$ hours. This has two contributions, relaxation that occurs during collisions of ^{3}He atoms due to dipole-dipole interactions [37], and relaxation that is presumably due largely to the interaction of the ^{3}He atoms with the walls. Finally, relaxation due to magnetic field inhomogeneities can probably be held to about $\Gamma_{\Delta B} = 1/100$ hours [38]. Collectively, under operating conditions, we would thus expect

$$\Gamma_R = \Gamma_{beam} + \Gamma_{cell} + \Gamma_{\Delta B} = 1/45 \text{ hours} + 1/50 \text{ hours} + 1/100 \text{ hours} = 1/19 \text{ hours}. \quad (14)$$

Thus, according to Eq. 10, the target polarization cannot be expected to exceed

$$P_{max} = \frac{\gamma_{SE}}{\gamma_{SE} + \Gamma_R} = 0.70. \quad (15)$$

Realistically, we will not achieve a Rb polarization of 100% in the pumping chamber, which will reduce the polarization to about 40-45%.

2. Target Cells

The construction and filling of the target cells must be accomplished with great care if $1/\Gamma_{cell}$ is to be in excess of 50 hours. We plan to use the "Princeton Prescription" which was developed for use in SLAC E-142. This resulted, among the cells that were tested, in lifetimes that were always better than 30 hours, and in about 60% of the cells, better than 50 hours. The following precautions will be taken:

- 1. Cells will be constructed from aluminosilicate glass.
- 2. All tubing will be "resized." This is a process in which the diameter of the tubing is enlarged by roughly a factor of two in order to insure a smooth pristine glass surface that is free of chemical impurities.
- 3. Cells will be subjected to a long (4–7 day) bake-out at high (> 400°C) temperature on a high vacuum system before filling.
- 4. Rb will be doubly distilled in such a manner as to avoid introducing any contaminants to the system.
- 5. The ^{3}He will be purified either by getters or a liquid ^{4}He trap during filling.

The cells will be filled to a high density of ^{3}He by maintaining the cell at a temperature of about 20 K during the filling process. This is necessary so that the *pressure* in the cell is below one atmosphere when the glass tube through which the cell is filled is sealed. The length of the cell will be 40 cm. The end windows will be collimated out of the spectrometer acceptance. The effective target length after collimation with be 20 cm. The end windows themselves will be about 100 μ thick. Thinner windows could in principle be used, but this does not appear to be necessary with collimation.

3. The Optics System

As mentioned above, approximately 50 Watts of "usable" light at 795 nm will be required. By "usable," we essentially mean light that can be readily absorbed by the Rb. It should be noted that the absorption line of the Rb will have a full width of several hundred GHz at the high pressures of ^{3}He at which we will operate. Furthermore, since we will operate with very high Rb number densities that are optically quite thick, quite a bit of light that is not within the absorption linewidth is still absorbed.

It is our plan to take advantage of new emerging diode laser technology to economically pump the target. Systems are now commercially available in which a single chip produces about 30 watts of light, about half of which is probably usable. Between 3–4 such systems should do the job. There is also a commercially available product which can produce 100 watts. While some studies of the use of diode lasers for spin-exchange optical pumping do exist in the literature [39], actual demonstrations of high polarizations in cells suitable for targets are much more recent [40]. For the recently finished SLAC experiment E154, the diode laser system was used for the spin exchange polarized ^{3}He target.

4. Polarimetry

Polarimetry will be accomplished by two means. During the experiment, polarization will be monitored using the NMR technique of adiabatic fast passage (AFP) [41]. The signals will be calibrated by comparing the ^{3}He NMR signals with those of water. The calibration will be independently verified by studying the frequency shifts that the polarized ^{3}He nuclei cause on the electron paramagnetic resonance (EPR) lines of Rb atoms. This second techniques will be performed in separate target studies, not during the experiment. For this experiment we will use the hadron HRS spectrometer as beam and target polarization monitor, the NMR technique of the target polarization measurement will be used as cross check.

5. Apparatus Overview

The target will be in air or, perhaps, in a helium bag. This greatly simplifies the design. The main components of the target include large Helmholtz coils that will be used to apply a static magnetic field of about 20 Gauss. In addition to establishing the quantization axis for the target, the coils are important for suppressing relaxation due to magnetic field inhomogeneities, which go like $1/B^2$. At 20 G, inhomogeneities can be as large as about 30 mG/cm while keeping $\Gamma_{\Delta B} < 1/100$ hours. By increasing the applied field to about 40 G,

and relaxing our requirements on $\Gamma_{\Delta B}$ by about factor of two, inhomogeneities as large as 0.25 G/cm can be tolerated. We are still finalizing our final choice of static field.

The NMR components in the target will include a set of RF drive coils, a separate set of pick-up coils, and appropriate electronics. The apparatus necessary for doing EPR polarimetry will include a small probe (housing a drive coil and a photodiode) and associated electronics. The polarimetry electronics will be controlled by a PC, which in turn will communicate with EPICS.

D. Proposed Measurements

The kinematics are chosen to cover the lowest Q^2 range possible with the Septum magnets. Two electron angles of 6° and 9° are chosen. Six incident electron energies will be used for each angle: 1.6, 2, 3, 4, 5 and 6 GeV. The scattered electron energies will cover from the threshold of the ^{3}He disintegration, through quasielastic peak and the resonance region, and into the deep inelastic region (here and throughout the text, the deep inelastic region is only refer to the region above the resonance region). Figure 6 shows the kinematical coverage for the proposed measurements.

The Hall A HRS electron spectrometer will be used for detecting the scattered electrons. The standard detector package setup will be sufficient for this experiment. The high resolution is needed for clear separation of the disintegration threshold from the elastic scattering. The hadron spectrometer will be used to monitoring the product of the beam and the target polarization by detecting the asymmetry of the elastically scattered electrons. The expected error on the product of the beam and target polarization is about 3%. The beam polarization and the target polarization will also be measured separately to provide a redundant check of the systematic errors. The target polarization will be monitored by NMR measurements. An uncertainty of less than $3-5\%$ in the target polarization is expected. The beam polarization will be measured with the Hall A Møller and/or the Compton polarimeters. An uncertainty of about 3% in the beam polarization is expected.

The virtual photon-nucleon longitudinal asymmetries (A_1) will be measured for all the kinematical settings to study the spin structure for the quasielastic, resonance and the deep inelastic regions. Experimentally, we will measure the target longitudinal asymmetry ($A_{\|}$) with target polarization parallel to the beam direction and the target transverse asymmetry ($A_{\perp}$) with target polarization perpendicular to the beam direction. The virtual photon-nucleon longitudinal asymmetry (A_1) is related to the experimental asymmetry as following:

$$A_1 = \frac{1}{P}\frac{2}{\sqrt{1-\epsilon^2}}(A_{\|}\cos\theta_q + A_{\perp}\sin\theta_q)(1+\epsilon R) \tag{16}$$

where P is the product of the beam polarization and the target polarization. $\epsilon = [1+2(q^2/Q^2)\tan(\theta/2)]^{-1}$, θ_q is the angle of the virtual photon with respect to the incident electron, $R = \sigma_L/\sigma_T$, is the ratio of the unpolarized longitudinal cross section to the transverse cross section.

To measure the GDH sum, two methods will be used. One is to use the asymmetries combining with the measured plus the existing cross sections to get the GDH sum. The other is to directly measure the cross section difference between the two helicity states.

$$\sigma_{TT'} = \frac{1}{P}\frac{1}{\sqrt{1-\epsilon^2}}(\Delta\sigma_{\parallel}\cos\theta_q + \Delta\sigma_{\perp}\sin\theta_q) \tag{17}$$

where $\Delta\sigma_{\parallel}(\Delta\sigma_{\perp})$ are the cross section difference of the two electron beam polarization states for target polarization parallel (perpendicular) to the beam direction. Both methods will be used and compared in the data analysis to obtain the best result for the GDH sum.

E. Count Rate and Beam Time Estimation

The cross sections for quasielastic, resonances and deep inelastic scattering are estimated using the code QFS [19]. Figure 7 shows the cross sections for incident energies of 4 GeV at scattering angle of 6° and 6 GeV at 9°. At most of the kinematical setting, the cross sections are very high. The counting rate will often be data acquisition speed limited. Asymmetries are estimated with the code AO [5] for the resonance region, and used E142 parametrization for the deep inelastic region (neglecting the Q^2 dependence). For the quasielastic peak, free nucleon form factors, along with the $P_{n(p)}$ of Friar [21], were used to estimate the asymmetries. The estimation of asymmetries was not used in rate and time estimation. They are listed in the table only to give us an idea how large asymmetries we are expecting. The time estimated are for 0.5% statistical error on the asymmetry for each momentum setting. The momentum bin is chosen to be about 4% of the momentum in most cases. Near the disintegration threshold and the pion threshold, we will make smaller binning to have better resolution. The statistical uncertainties in the asymmetry is

$$\delta_{stat}(A(E)) \approx \frac{1}{Pf\sqrt{Tc}} \tag{18}$$

where P is the product of electron beam and target polarizations, f is the target dilution factor, T is the counting time and c is the counting rate

$$c = L \times \sigma \times \epsilon\Delta\Omega\Delta E' \tag{19}$$

where L is the luminosity, σ is the unpolarized cross section, $\Delta\Omega$ and $\Delta E'$ are the solid angle acceptance of the spectrometer and the energy bin, and ϵ includes all the correction factors, the main one matters for the estimation is the radiative correction factor. Table 5 lists the kinematical settings with the counting rates and the estimated beam time for all the data taking. In the rate and time estimation, the following assumption were made:

Effective target length:	20 cm (end windows are collimated out)
Target density:	$2.5 \times 10^{20}(atoms/cm^3)$
Beam Current:	1-15 μA
Luminosity L:	5×10^{35} $(cm^{-2}s^{-1})$
Solid angle $\Delta\Omega$:	3.7 msr
Momentum Acceptance ΔP:	8%
Energy bin $\Delta E'$:	$< 4\%$ E'
Efficiency ϵ:	0.7
Beam polarization:	80%
Target polarization:	40%
Dilution factor:	0.3

Table 5. Kinematics, Rates and Estimated Beam Time

Table 5a. $\theta = 6°$, E=6.045 GeV

E'(GeV)	ν(GeV)	Q^2(GeV^2)	x	ϵ	$A_{\|\|}$	Rate(Hz)	Time(Hours)
4.000	2.045	0.265	0.069	0.916	-0.0870	3317.4	0.73
3.600	2.445	0.238	0.052	0.875	-0.0750	2556.9	0.94
3.200	2.845	0.212	0.040	0.823	-0.0630	2020.1	1.19
2.800	3.245	0.185	0.030	0.759	-0.0520	1631.2	1.48
2.400	3.645	0.159	0.023	0.683	-0.0420	1340.4	1.80
2.000	4.045	0.132	0.017	0.594	-0.0330	1117.6	2.16
1.600	4.445	0.106	0.013	0.493	-0.0260	945.0	2.55

Table 5b. $\theta = 6°$, E=5.045 GeV

E'(GeV)	ν(GeV)	Q^2(GeV^2)	x	ϵ	$A_{\|\|}$	Rate(Hz)	Time(Hours)
4.000	1.045	0.221	0.113	0.968	-0.0011	5000.0	0.48
3.700	1.345	0.205	0.081	0.949	-0.0056	5000.0	0.48
3.400	1.645	0.188	0.061	0.922	-0.0810	4505.9	0.54
3.100	1.945	0.171	0.047	0.887	-0.0700	3517.8	0.69
2.800	2.245	0.155	0.037	0.844	-0.0590	2802.5	0.86
2.500	2.545	0.138	0.029	0.792	-0.0490	2274.8	1.06
2.200	2.845	0.122	0.023	0.729	-0.0410	1875.3	1.29
1.900	3.145	0.105	0.018	0.657	-0.0330	1566.6	1.54
1.600	3.445	0.088	0.014	0.574	-0.0270	1324.4	1.82
1.300	3.745	0.072	0.010	0.481	-0.0220	1135.0	2.12

Table 5c. $\theta = 6°$, E=4.045 GeV

E'(GeV)	ν(GeV)	Q^2(GeV^2)	x	ϵ	$A_{\|\|}$	Rate(Hz)	Time(Hours)
3.845	0.200	0.170	0.454	0.993	-0.0012	5000.0	4.00
3.595	0.450	0.159	0.189	0.988	-0.0420	5000.0	2.00
3.345	0.700	0.148	0.113	0.977	-0.0026	5000.0	0.48
3.095	0.950	0.137	0.077	0.960	-0.0010	5000.0	0.48
2.845	1.200	0.126	0.056	0.936	-0.0008	5000.0	0.48
2.595	1.450	0.115	0.042	0.904	-0.0004	5000.0	0.48
2.345	1.700	0.104	0.033	0.863	-0.0540	4098.0	0.59
2.095	1.950	0.093	0.025	0.813	-0.0450	3248.9	0.74
1.845	2.200	0.082	0.020	0.752	-0.0370	2617.9	0.92
1.595	2.450	0.071	0.015	0.679	-0.0300	2139.2	1.13
1.345	2.700	0.060	0.012	0.596	-0.0240	1773.2	1.36
1.095	2.950	0.049	0.009	0.502	-0.0180	1496.7	1.61

Table 5d. $\theta = 6°$, E=3.045 GeV

E'(GeV)	ν(GeV)	Q^2(GeV^2)	x	ϵ	$A_{\|\|}$	Rate(Hz)	Time(Hours)
2.895	0.150	0.097	0.343	0.993	-0.0011	5000.0	4.00
2.695	0.350	0.090	0.137	0.987	-0.0710	5000.0	2.00
2.495	0.550	0.083	0.081	0.975	-0.0070	5000.0	1.00
2.295	0.750	0.077	0.054	0.956	-0.0016	5000.0	0.48
2.095	0.950	0.070	0.039	0.929	-0.0010	5000.0	0.48
1.895	1.150	0.063	0.029	0.893	-0.0008	5000.0	0.48
1.695	1.350	0.057	0.022	0.846	-0.0004	5000.0	0.48
1.495	1.550	0.050	0.017	0.787	-0.0330	4100.1	0.59
1.295	1.750	0.043	0.013	0.717	-0.0260	3254.3	0.74
1.095	1.950	0.037	0.010	0.634	-0.0210	2632.7	0.92
0.895	2.150	0.030	0.007	0.539	-0.0160	2180.5	1.11
0.695	2.350	0.023	0.005	0.432	-0.0120	1875.2	1.29

Table 5e. $\theta = 6°$, E=2.045 GeV

E'(GeV)	ν(GeV)	Q^2(GeV^2)	x	ϵ	$A_{\|\|}$	Rate(Hz)	Time(Hours)
1.945	0.100	0.044	0.232	0.993	-0.0010	5000.0	4.00
1.795	0.250	0.040	0.086	0.986	-0.0210	5000.0	2.00
1.645	0.400	0.037	0.049	0.971	-0.0380	5000.0	1.00
1.495	0.550	0.033	0.032	0.948	-0.0053	5000.0	0.48
1.345	0.700	0.030	0.023	0.913	-0.0018	5000.0	0.48
1.195	0.850	0.027	0.017	0.867	-0.0010	5000.0	0.48
1.045	1.000	0.023	0.012	0.806	-0.0011	5000.0	0.48
0.895	1.150	0.020	0.009	0.731	-0.0007	5000.0	0.48
0.745	1.300	0.017	0.007	0.640	-0.0004	4111.9	0.59
0.595	1.450	0.013	0.005	0.534	-0.0003	3401.0	0.71
0.445	1.600	0.010	0.003	0.414	-0.0080	3002.0	0.80
0.295	1.750	0.007	0.002	0.282	-0.0050	2944.0	0.82

Table 5f. $\theta = 6°$, E=1.645 GeV

E'(GeV)	ν(GeV)	Q^2(GeV^2)	x	ϵ	$A_{\|\|}$	Rate(Hz)	Time(Hours)
1.575	0.070	0.028	0.216	0.994	-0.0800	5000.0	4.00
1.475	0.170	0.027	0.083	0.989	-0.0010	5000.0	2.00
1.375	0.270	0.025	0.049	0.979	-0.0360	5000.0	1.00
1.275	0.370	0.023	0.033	0.963	-0.0450	5000.0	0.48
1.175	0.470	0.021	0.024	0.941	-0.0120	5000.0	0.48
1.075	0.570	0.019	0.018	0.911	-0.0038	5000.0	0.48
0.975	0.670	0.018	0.014	0.873	-0.0020	5000.0	0.48
0.875	0.770	0.016	0.011	0.825	-0.0012	5000.0	0.48
0.775	0.870	0.014	0.009	0.767	-0.0009	5000.0	0.48
0.675	0.970	0.012	0.007	0.699	-0.0011	5000.0	0.48
0.575	1.070	0.010	0.005	0.620	-0.0010	5000.0	0.48
0.475	1.170	0.009	0.004	0.531	-0.0006	4437.8	0.54

Table 5g. $\theta = 9°$, E=6.045 GeV

E'(GeV)	ν(GeV)	Q^2(GeV^2)	x	ϵ	$A_{\parallel}$	Rate(Hz)	Time(Hours)
4.000	2.045	0.595	0.155	0.910	-0.1000	769.9	3.13
3.600	2.445	0.536	0.117	0.869	-0.1030	622.8	3.87
3.200	2.845	0.476	0.089	0.818	-0.0940	504.4	4.78
2.800	3.245	0.417	0.068	0.755	-0.0870	413.4	5.83
2.400	3.645	0.357	0.052	0.679	-0.0740	343.3	7.02
2.000	4.045	0.298	0.039	0.591	-0.0620	288.7	8.35
1.600	4.445	0.238	0.029	0.490	-0.0490	246.1	9.80

Table 5h. $\theta = 9°$, E=5.045 GeV

E'(GeV)	ν(GeV)	Q^2(GeV^2)	x	ϵ	$A_{\parallel}$	Rate(Hz)	Time(Hours)
4.000	1.045	0.497	0.253	0.962	-0.0007	1626.7	1.48
3.700	1.345	0.460	0.182	0.942	-0.0012	1376.4	1.75
3.400	1.645	0.422	0.137	0.916	-0.1050	1083.1	2.23
3.100	1.945	0.385	0.106	0.882	-0.1020	877.3	2.75
2.800	2.245	0.348	0.083	0.839	-0.0970	716.6	3.36
2.500	2.545	0.311	0.065	0.787	-0.0880	589.6	4.09
2.200	2.845	0.273	0.051	0.725	-0.0770	490.4	4.92
1.900	3.145	0.236	0.040	0.653	-0.0630	412.5	5.84
1.600	3.445	0.199	0.031	0.571	-0.0520	351.0	6.87
1.300	3.745	0.161	0.023	0.479	-0.0410	302.4	7.97

Table 5i. $\theta = 9°$, E=3.045 GeV

E'(GeV)	ν(GeV)	Q^2(GeV^2)	x	ϵ	$A_{\parallel}$	Rate(Hz)	Time(Hours)
2.895	0.150	0.217	0.771	0.987	-0.0013	5000.0	4.00
2.695	0.350	0.202	0.308	0.980	-0.0230	5000.0	2.00
2.495	0.550	0.187	0.181	0.969	-0.0110	4893.6	1.00
2.295	0.750	0.172	0.122	0.950	-0.0019	3385.2	0.71
2.095	0.950	0.157	0.088	0.923	-0.0010	2606.0	0.93
1.895	1.150	0.142	0.066	0.887	-0.0011	1990.8	1.21
1.695	1.350	0.127	0.050	0.840	-0.0005	1490.8	1.62
1.495	1.550	0.112	0.039	0.783	-0.0610	1154.7	2.09
1.295	1.750	0.097	0.030	0.713	-0.0500	921.2	2.62
1.095	1.950	0.082	0.022	0.630	-0.0410	746.9	3.23
0.895	2.150	0.067	0.017	0.536	-0.0320	614.9	3.92
0.695	2.350	0.052	0.012	0.430	-0.0240	518.3	4.65

Table 5j. $\theta = 9°$, E=1.645 GeV

E'(GeV)	ν(GeV)	Q^2(GeV^2)	x	ϵ	$A_{\|\|}$	Rate(Hz)	Time(Hours)
1.575	0.070	0.064	0.486	0.987	-0.0014	5000.0	4.00
1.475	0.170	0.060	0.187	0.982	-0.0010	5000.0	2.00
1.375	0.270	0.056	0.110	0.972	-0.0270	5000.0	1.00
1.275	0.370	0.052	0.074	0.957	-0.0630	5000.0	1.00
1.175	0.470	0.048	0.054	0.935	-0.0150	5000.0	0.48
1.075	0.570	0.044	0.041	0.905	-0.0045	4268.4	0.56
0.975	0.670	0.039	0.031	0.867	-0.0021	3447.6	0.70
0.875	0.770	0.035	0.025	0.820	-0.0013	2884.9	0.84
0.775	0.870	0.031	0.019	0.763	-0.0010	2230.1	1.08
0.675	0.970	0.027	0.015	0.695	-0.0011	1788.2	1.35
0.575	1.070	0.023	0.012	0.617	-0.0010	1487.7	1.62
0.475	1.170	0.019	0.009	0.528	-0.0006	1250.3	1.93

With the estimated beam time, the statistic uncertainties in the sum rules range from 2μb at $Q^2 = 0.02(GeV/c)^2$ to less than 0.1μb at $Q^2 = 0.5(GeV/c)^2$. In the sum rule measurements, the systematic uncertainties will dominate.

Figure 8 shows the expected results for the GDH sum rule measurements. The error bars are the statistic and systematic errors added in quadrature. Also shown in the figure are the resonance saturation model calculation (AO code) [5] and the Chiral Perturbation Theory calculation [18].

The beam time needed for the measurements and overhead are listed in Table 6. The time needed for transverse asymmetry measurements is assumed to be about 30% of the time needed for longitudinal asymmetry measurements. The total beam time requested is 16 days.

Table 6. Beam Time Request (Hours)

$A_{\|\|}$ 6°	73
$A_{\|\|}$ 9°	129
$A_{\perp}$ 6°	22
$A_{\perp}$ 9°	40
Total Data Taking	264
Calibrations	48
Energy/Angle Changes	20
Momentum Changes	32
Polarization Changes	20
Total Overhead	120
Grand Total	384

III. SYSTEMATIC UNCERTAINTIES

For the sum rule measurements, due to the $1/\nu$ weighting in the integral, the uncertainty requirements are not as stringent as they may appear to be. The systematic uncertainty in the total GDH sum (I) can be related to the uncertainty in each energy bin:

$$\delta_{sys} I = \delta_{sys}(\Delta\sigma) \ln \frac{\nu_{max}}{\nu_{min}} \tag{20}$$

where $\nu_{min} \approx 5.9$ MeV and ν_{max} is the maximum energy loss we can reach for each constant Q^2.

For the asymmetry measurements, some of the systematic uncertainties will largely cancel while some others, which are helicity dependent, will not cancel.

The systematic uncertainties will be dominated by the target and beam polarization measurements, and the radiative tail corrections. The radiative tail will be discussed in the next section. The target and the beam polarization will be separately measured and will also be monitored with the elastic measurements. We expect the combined polarization uncertainty to be about 3% using the elastic measurements method.

IV. EXPERIMENTAL CONSIDERATION

In this section, we would like to address a few issues that are important for the proposed experiment.

A. Radiative tails

Radiative tails for all the kinematical settings were calculated. The target material, the glass cell wall, the beam pipe windows and the spectrometer window are all included in the calculation. Figure 7 shows the results for incident energies of 4 GeV at scattering angle of 6° and 6 GeV at 9° along with the cross sections calculated with the QFS code. The radiative tail contribution decreases with increasing incident energy. We will not run with energy less than 1.6 GeV to avoid too large a contribution from the radiative tails.

B. Background And Normalization

The largest background comes from the process ^{3}He(e,π^-). Cross sections for this process were calculated for all our kinematics. In the worst case at incident energy of 6 GeV at 9° (see Figure 7b), the π cross section is still a factor of several less than electron cross section. With the excellent particle identification detectors in the HRS spectrometers, The π background is not an issue.

Since we would like to measure cross sections as well as the asymmetries, absolute normalization is necessary. We will measure ^{3}He elastic cross sections at each incident energy setting for normalization.

C. Nuclear effect for ^{3}He

The GDH sum rule and its Q^2 dependence for ^{3}He itself is of great interest. However, at the same time, we can also extract information on the neutron. To extract the sum rule for the neutron from the measured data for the ^{3}He, we need to take into account the fact that the polarized ^{3}He is only approximately a polarized neutron target [20] [21]. We need

to subtract the contribution from the small proton polarization and take into account that the neutron is not polarized to the same level as the ^{3}He itself.

The first order correction can be made by using the calculation of Friar *et al.* [21] that the proton is about 3% polarized in the opposite direction from the ^{3}He polarization, while the neutron is about 87% polarized along the ^{3}He polarization direction.

Recently degli Atti *et. al.* [22] suggested to use the following equation to extract neutron sum rules:

$$\tilde{I}^n(Q^2) = \frac{1}{p_n}[I^{^3He}(Q^2) - 2p_p I^p(Q^2)] \tag{21}$$

where $p_{n(p)}$ is the effective nucleon polarization, produced by the S' and D waves in the ground state of ^{3}He. It was shown that, even though the quantity $\tilde{g}_1^n(x,Q^2)$ differs significantly from $g_1^n(x,Q^2)$ at the resonance region at low Q^2, the difference for the integrated quantity $\tilde{I}^n(Q^2)$ does not differ much from the free neutron sum rule $I^n(Q^2)$ (at most 10%). Figure 9 shows the comparison of the extracted neutron sum rule using equation (20) with the free neutron sum rule (generated from Burkert and Li's model).

More realistic ^{3}He models can be used to further study the ^{3}He GDH sum rule. Several theorists are investigating this problem [23].

Another effect will contribute to the systematic uncertainties is the Fermi motion, which extends the quasi-elastic tail into the inelastic region and causes some uncertainty in the determination of the lower limit of the integration for the neutron GDH sum rule. This effect is small at lower energies and increases as energy increases. The uncertainty due to this effect is estimated to be not significant in most cases.

It is worth while to point out that in this experiment we will have measurements to directly study the ^{3}He model by comparing the difference of the GDH sum rule for the ^{3}He and the neutron with the measurements from the disintegration threshold to the pion threshold. The contribution to the GDH sum rule from the disintegration threshold to the pion threshold should be approximately equal to the difference of the ^{3}He sum rule to the neutron sum rule, if the assumption that the polarized ^{3}He target is almost a polarized neutron target is valid. So the measurement from the disintegration threshold to the pion threshold can be used to study how good the polarized ^{3}He target is a polarized neutron target.

V. SUMMARY

With the future addition of the septum magnets in Hall A, angles as small as 6° will be accessible. Making full use of the small angle capability, we propose to measure asymmetries of the polarized electron scattering off the polarized ^{3}He target to very small Q^2 range (from 0.02 to 0.5 $(GeV/c)^2$). GDH sum rule and its Q^2 dependence will be studied for both ^{3}He and the neutron at this very low Q^2 range. The slope at Q^2 near zero will be measured and extrapolation to the real photon point can be performed. The comparison of the ^{3}He with neutron will be used to study the ^{3}He model. The asymmetries at the threshold, the quasielastic and the resonance region will provide a powerful tool to study and constrain the theoretical models. The total beam time requested for the measurements is 16 days.

REFERENCES

[1] S. B. Gerasimov, Yad. Fiz. **2**, 839 (1965).
S. D. Drell and A. C. Hearn, Phys. Rev. Lett. **162**, 1520 (1966).
[2] F. E. Low, Phys. Rev. 96,1428(1954).
M. Gell-Mann, M. Goldberger and W. Thirring, Phys. Rev. **95** 1612 (1954).
[3] I. Karliner, Phys. Rev. **D 7** 2717 (1973).
[4] R. L. Workman and R. A. Arndt, Phys. Rev. **D 45** 1789 (1992).
[5] V. Burkert and Zh. Li, Phys. Rev. **D 47** 46 (1993).
[6] A. M. Sandorfi, C. S. Whisnant and M. Khandaker, Phys. Rev. **D 50** 6681 (1994).
[7] S. D. Bass, HEP-PH/9703254, 9601244; S. D. Bass, Modern Phys. Lett. A12, 1051 (1997); H.-W. Hammer, D. Drechsel and T. Mart, NUCL-TH/9701008.
[8] L. N. Chang, Y. Liang and R. L. Workman, Phys. Lett. **B329**, 514 (1994).
[9] M. Ansemino, B. L. Ioffe and E. Leader, Sov. J. Nucl. Phys.
[10] V. Burkert and B. L. Ioffe, Phys. Lett. **B296**,223 (1992).
V. Burkert and B. L. Ioffe, JETP 105,1153 (1994); **49**,136 (1989).
D. Drechsel, nucl-th/9411034 (1994).
[11] J. Ashman et al., Nucl. Phys. **B 328** 1 (1989).
[12] G. Baum *et al.*, phys. Rev. Lett. **45**, 2000(1980); **51**,1135(1983)
[13] B. Adeva et al., Phys. Lett. **B396**,338(1997); **B 320** 400 (1994); **B 329**, 399(1994).
[14] P. L. Anthony *et al.*, Phys. Rev. Lett. **71**,959(1993);
K. Abe *et al.*, Phys. Rev. Lett **74** , 346 (1995); **75**, 25 (1985); **78**, 815(1997) Phys.Lett.**364**, 61 (1995);
K. Abe *et al.*, Phys. Rev. Lett (1997) O. Randon, private communication (1997)
[15] K. Ackerstaff *et al.*, hep-ex/9703005 .
[16] Bates Proposal 88-23, D. Beck, Spokesperson.
[17] A. Afanasev, J. Goity, *private communication.*
[18] V. Bernard, N. Kaiser, and U-G. Meissner Phys.Rev. **D48** 3062 (1993).
[19] J.W. LIGHTBODY JR. AND J.S. O'CONNELL, Computers in Physics, 1988
[20] S. J. Brodsky and J. R. Primack, Ann. Phys. **52**, 315(1969)
[21] J. Friar *et al.*, Phys. Rev. **C42**, 2310(1990)
[22] C. Ciofi degli Atti and S. Scopetta, nucl-th/9606034 (1996).
[23] R. Schiavilla, *private communication*; J. Carlson, *private communication*; J. Golak, *private communication.*
[24] TJNAF proposal E91-015, D. Sober, spokesperson.
[25] TJNAF proposal E94-117, J. P. Chen, S. Gilad, C. Whisnant, spokespersons.
[26] LEGS-Spin-Collaboration, BNL-61005 (1994)
[27] J. Arends *et al.*, Proposal to measure the GDH sum rule, Bonn and Mainz (1993)
[28] J.-P. Didelez, private communication.
[29] TJNAF proposal E91-023, V. Burkert, D. Crabb and R. Minehart, spokespersons.
[30] TJNAF proposal E93-009, S. E. Kuhn, spokesperson.
[31] TJNAF proposal E94-010, G. Cates, Z. Meziani, spokespersons.
[32] A proposal for two septum magnets for forward angle physics in Hall A
[33] TJNAF proposal E94-107, F. Garibaldi, J. LeRose, P. Markowitz, T. Saito, Spokespersons.

[34] M. A. Bouchiat, T. R. Carver and C. M. Varnum, Phys. Rev. Lett. **5**,373 (1960)
N. D. Bhaskar, W. Happer, and T. McClelland, Phys. Rev. Lett. **49**, 25 (1982)
W. Happer *et al.*, Phys. Rev. **A29**, 3092(1984)
[35] T.E. Chupp *et al.*, Phys. Rev. **C36**, 2244(1987)
[36] K. P. Coulter *et al.*, Nucl. Inst. Meth. in Phys. Res. **A276**, 29(1989)
[37] N. R. Nersbury *et al.*, Phys. Rev. **A48**, 4411 (1993)
[38] G. D. Cates *et al.*, Phys. Rev. **A38**,5092 (1988)
[39] M. E. Wagshul and T. E. Chupp, Phys. Rev. **A40**, 4447(1989)
[40] Private communication, B. Cummings (1994)
[41] A. Abragam, *Principles of Nuclear Magnetism* (Oxford University Press, New York, 1961).

Figure Captions

- Figure 1: Schematic layout of the modifications to the HRS setup .
- Figure 2: Layout of the Septum insertion.
- Figure 3: Stray field generated near the target region.
- Figure 4: Layout of the system at 6 degree. The Septum is shown at 70 cm and the the corrector coils (CC) are shown at -10 cm. All angles are in degrees and minutes.
- Figure 5: Schematics of the spin-exchange polarized ^{3}He target.
- Figure 6: Kinematical coverage. The solid line connects the ends of all the lines is the elastic limit. The six solid curves are for scattering angles of 6° with incident energies of 1.6, 2, 3, 4, 5 and 6 GeV (from the lowest to the highest solid curves). The four dashed curves are for scattering angles of 9° with incident energies of 1.6, 3, 5 and 6 GeV (from the lowest to the highest dashed curves). The dotted lines are the acceptance limits for the lowest energy setting for 6° and the highest energy setting for 9°.
- Figure 7: Top figure (6a) is for incident energy of 4 GeV and scattering angle of 6°; bottom figure (6b) is for incident energy of 6 GeV and 9°. Solid curves are ^{3}He(e,e') cross sections calculated with code QFS [19]; Dashed curves are the radiative tails; Dotted curves are ^{3}He(e,π) cross sections calculated with code EPC [19].
- Figure 8: Expected results for GDH sum for neutron. The solid curve is the calculation of a resonance saturation model by Burkert and Li [5]. The dashed curve is the same model renormalized to the GDH at the real photo point. The solid line is the prediction of the slope at real photon point by a Chiral Perturbation Theory [18].
- Figure 9: Comparison of extracted neutron GDH sum (crosses) with the free neutron GDH sum (full curve) and the ^{3}He GDH sum (dots). The free neutron GDH sum is from the Burkert and Li/citeBL model. The ^{3}He GDH sum is constructed from the free neutron and proton spin structure functions with a prescription given in the ref. [22]. The extracted neutron GDH sum uses the equation (20).

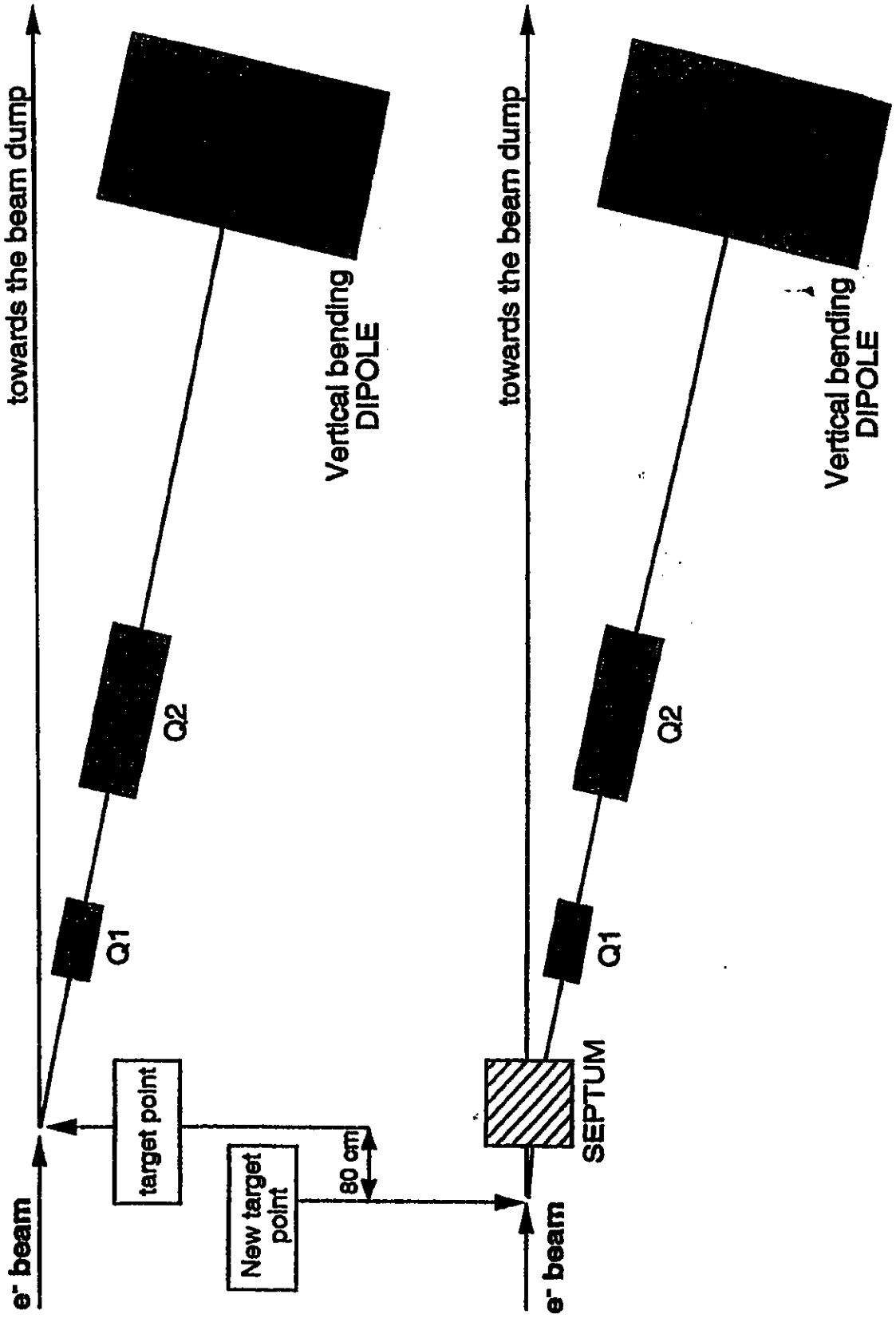

Figure 1: Schematic Layout of the proposed modifications to the HRS setup

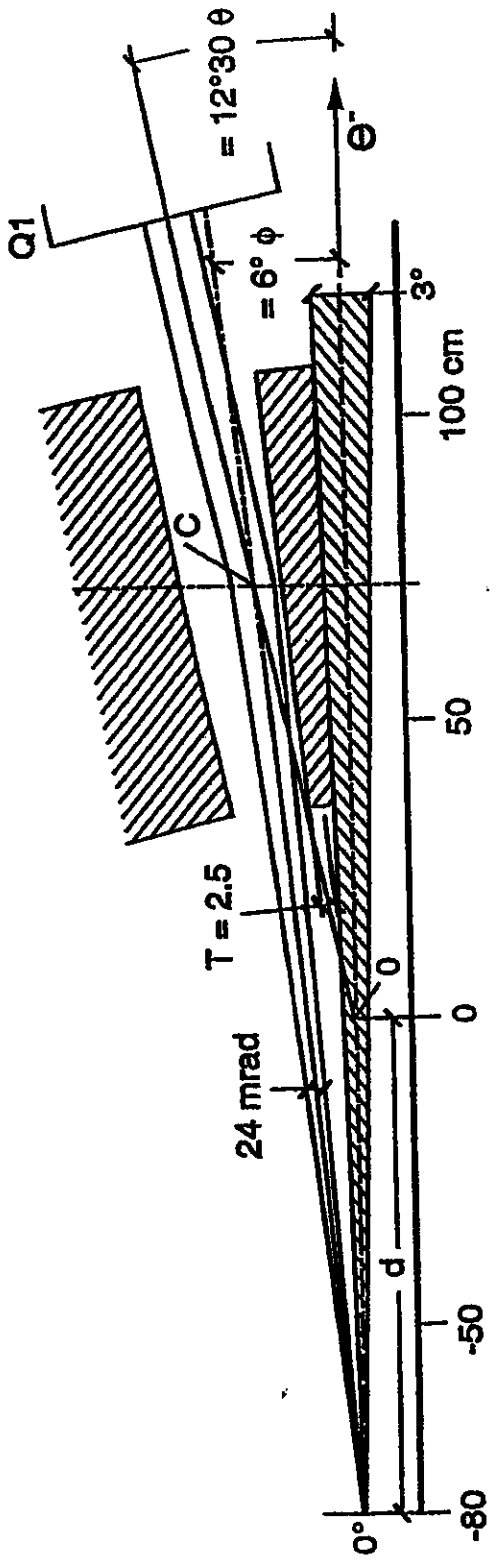

Figure 2: Layout of the septum insertion

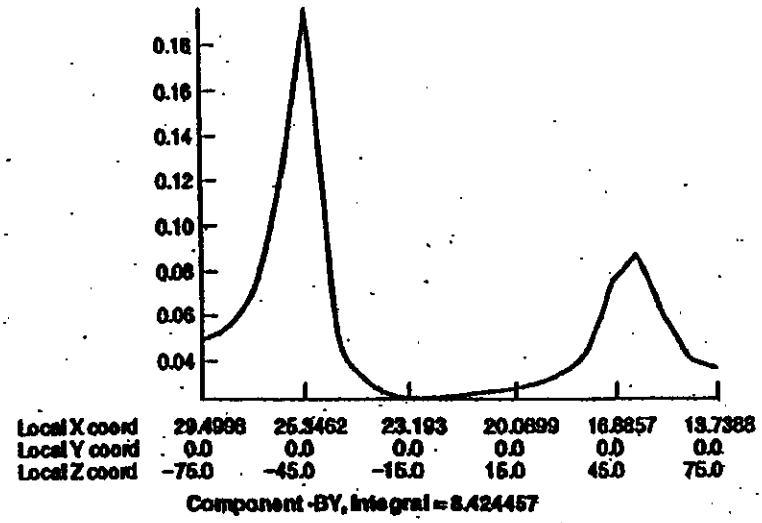

Figure 3 : Stray field generated on the beam pipe in the case 6 degrees

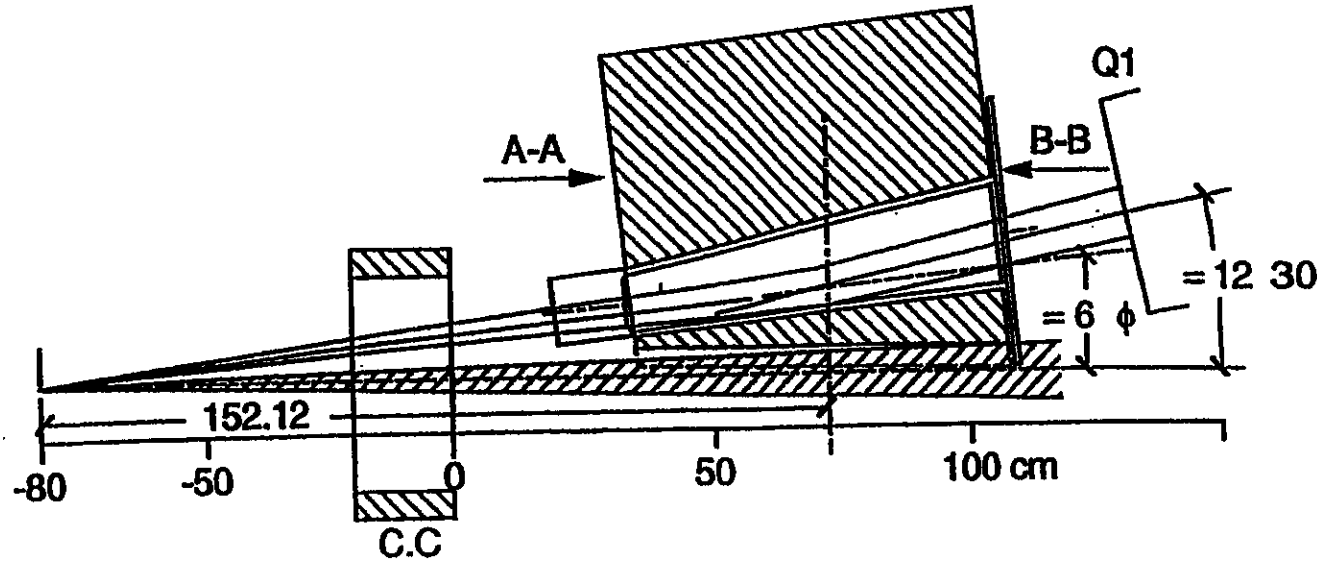

Figure 4: Layout of the system in the "extreme" angular conditions. The septum is shown at 70 cm and the corrector coils (CC) are shown at -10 cm. All angles are in degrees and minutes.

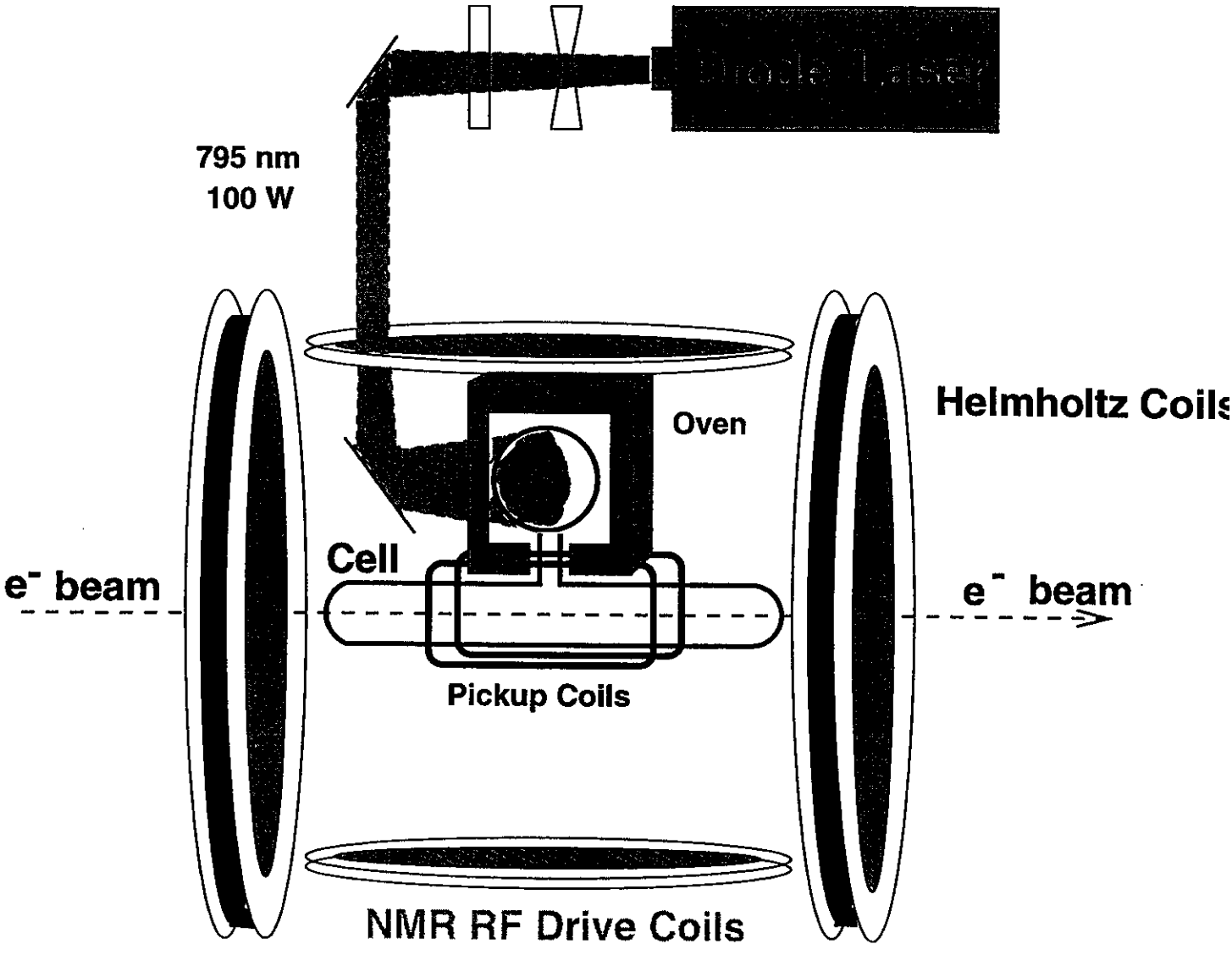

FIG. 5. Schematics of the spin-exchange polarized ^{3}He target.

Figure 6, Kinematics

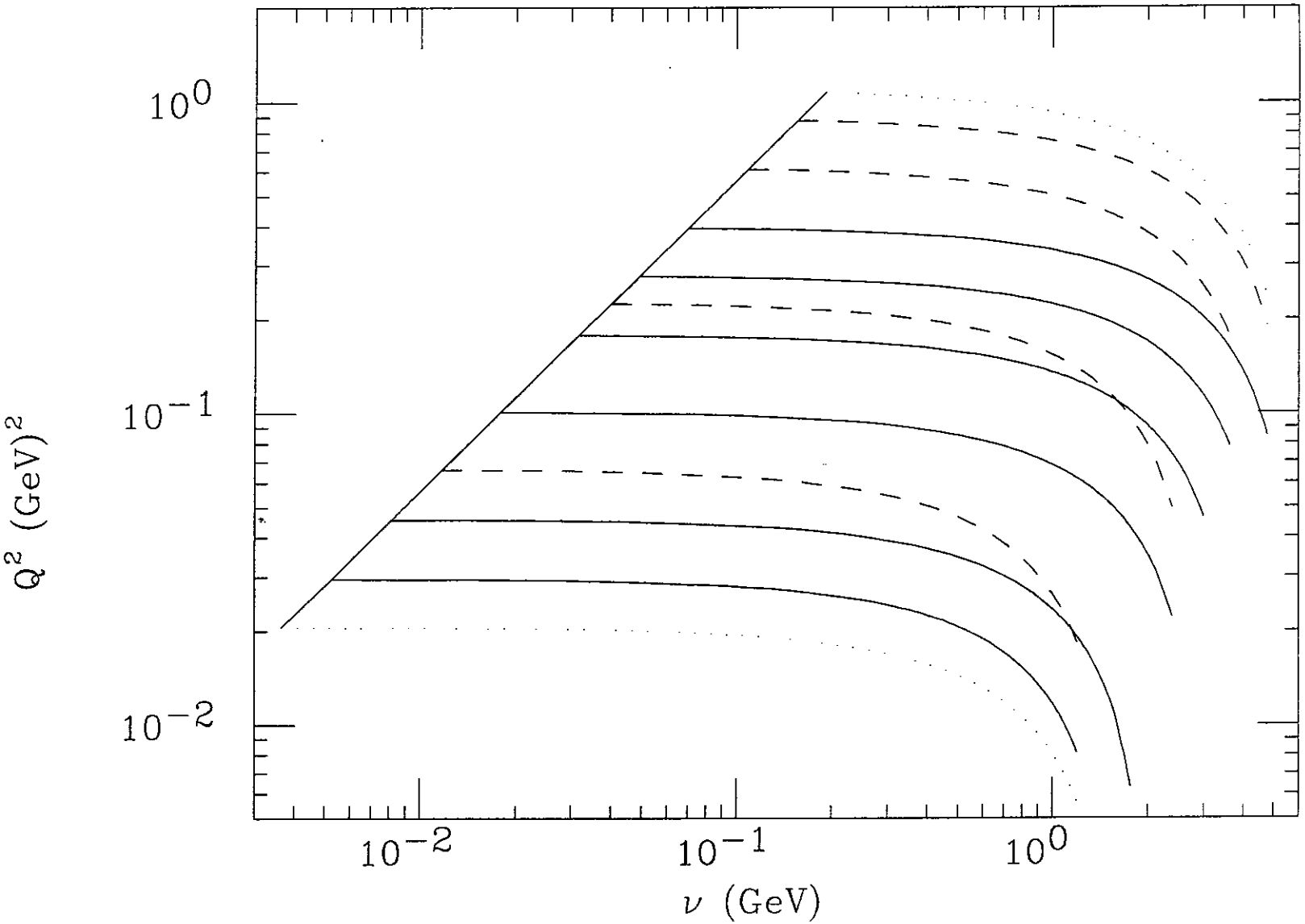

Figure 7a, 4 GeV, 6°

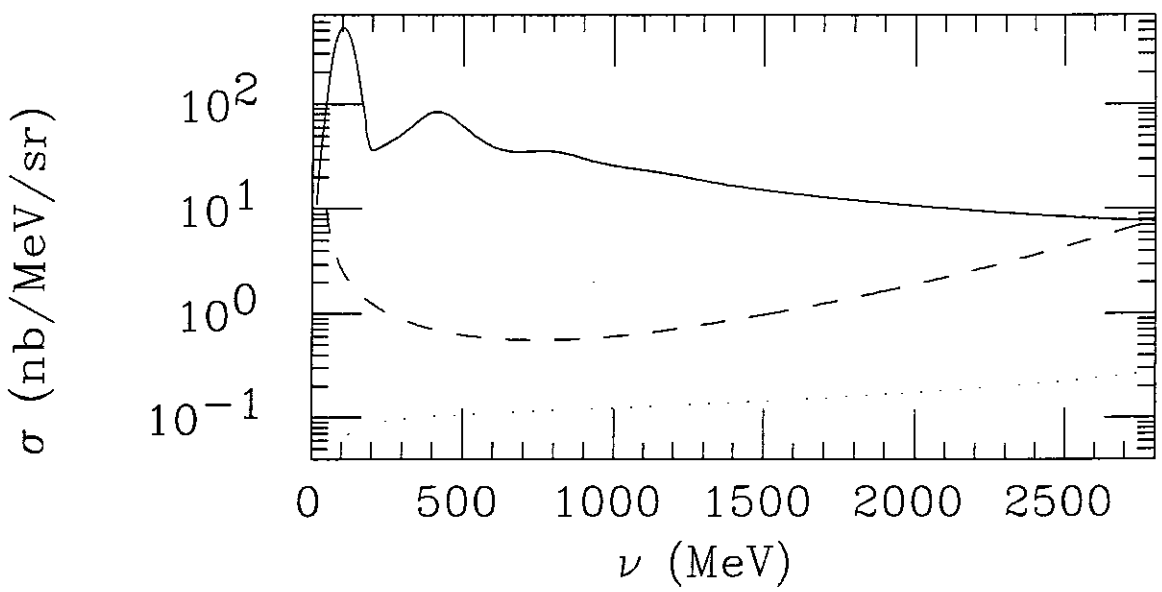

Figure 7b, 6 GeV, 9°

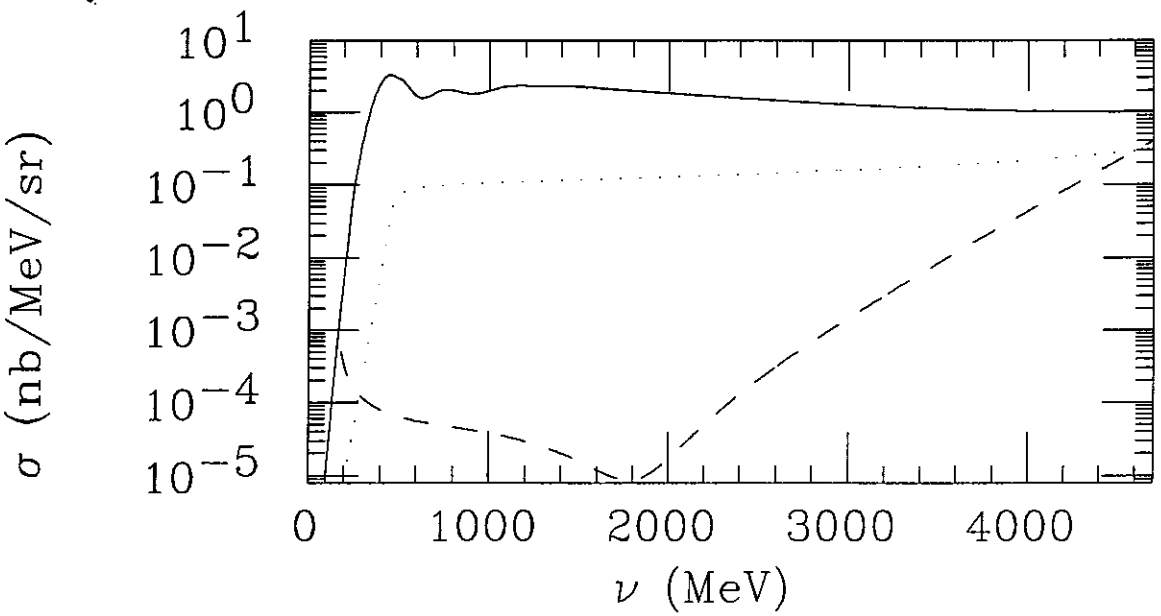

Figure 8, Expected Results on GDH(n)

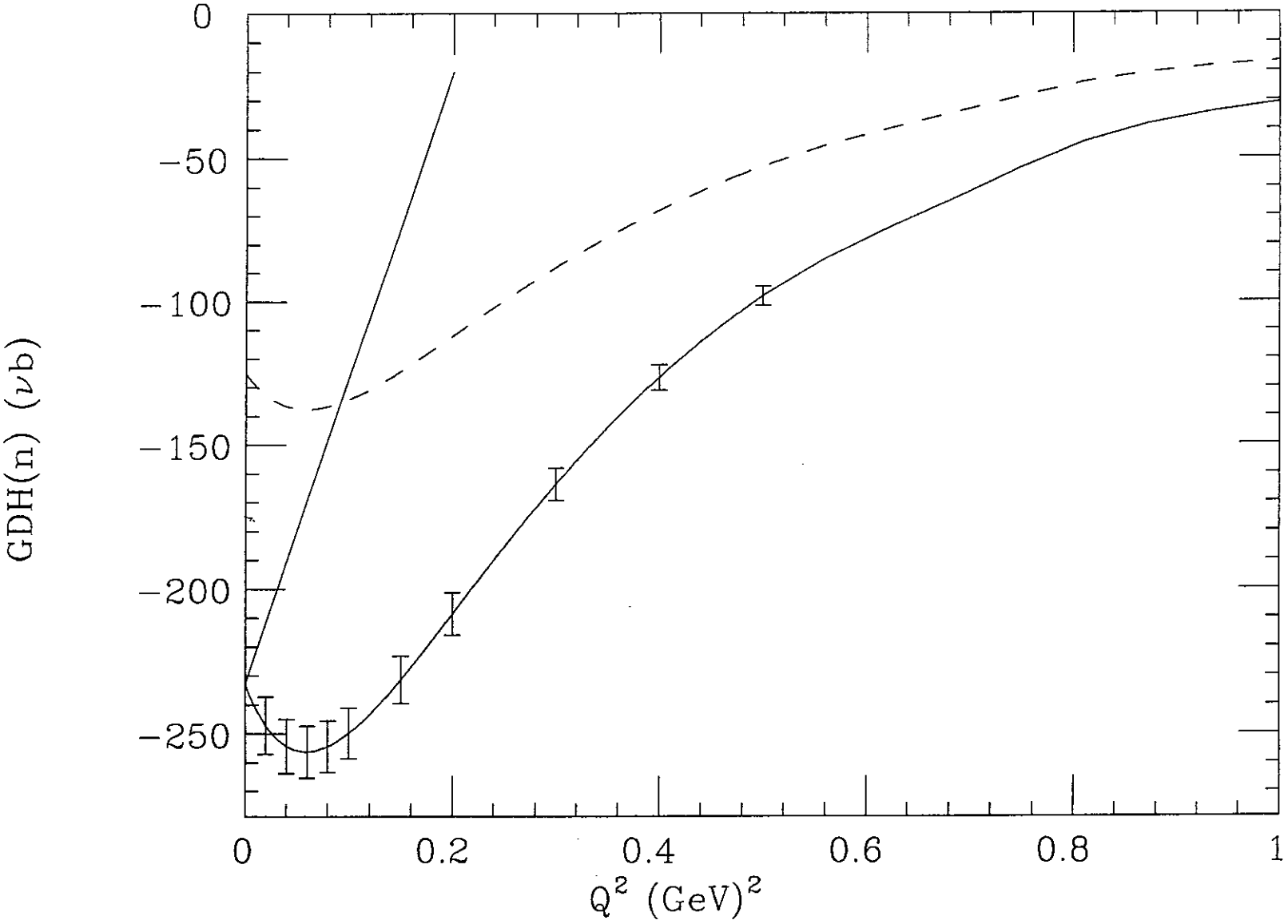

Figure 9: Comparison of extracted neutron GDH sum (crosses) with the free neutron GDH sum (full curve) and the ^{3}He GDH sum (dots).